Experimental evaluation of phase and velocity control for a cyclorotor wave energy converter

Andrei Ermakov, Florent Thiebaut, and John V. Ringwood

***Abstract*—The research presented in the paper is dedicated to the analysis of the 3D experimental testing results of a 1:20 scale prototype LiftWEC cyclorotor wave energy converter (WEC). The scaled prototype was built and tested in the Hydraulic and Offshore Engineering wave Tank (HOET) by Ecole Centrale Nantes (ECN) in 2022. The analysis is conducted using the analytical control-oriented point-vortex model. The presented research covers a range of tests, with particular focus on cases where positive mechanical power generation has been recorded. The analysis of such cases is important, in highlighting the conditions needed for optimum energy conversion, for future development of cyclorotor WEC technology. The study also reviews the results of tests where the rotor rotational speed is varied within each period of monochromatic waves. This is the first experimental test of such a control strategy for cyclorotor WECs.**

***Index Terms*—Cyclorotor, Efficiency, Control, Wave Energy Converters, LiftWEC, Experimental Results**

I. Introduction

Cyclorotor based wave energy converter (WEC) technology [1], [2] has reached some level of maturity with technology readiness level (TRL) four reached during the LiftWEC project [3] and TRL six for the Atargis project [4]. The recent results reported in publications [5]–[9] and project deliverables [10], [11] highlight many benefits of this alternative to more traditional [12] wave energy extraction technology.

Cyclorotor extract wave energy due to the interaction between hydrofoils and water particle circulation caused by wave propagation. The lift forces generated on hydrofoils accelerate the rotor rotation, inducing torque on the main shaft. This torque can be absorbed by a rotational (unidirectional) generator [1], [13], [14]. The rotor is designed to avoid significant structural loads and allow survival in harsh ocean environments [15], [16]. Cyclorotors can also be installed on various marine structures (Fig. 1). The benefits derived from cyclorotor WEC technology allow the prediction of the levelized cost of energy (LCoE) for the spar-buoy LiftWEC configuration with TRL4 (Fig. 1b) at $\sim$ 140 €/MWh [10]. Such a relatively small LCoE value is comparable with the LCoE generated by offshore wind platforms [17].

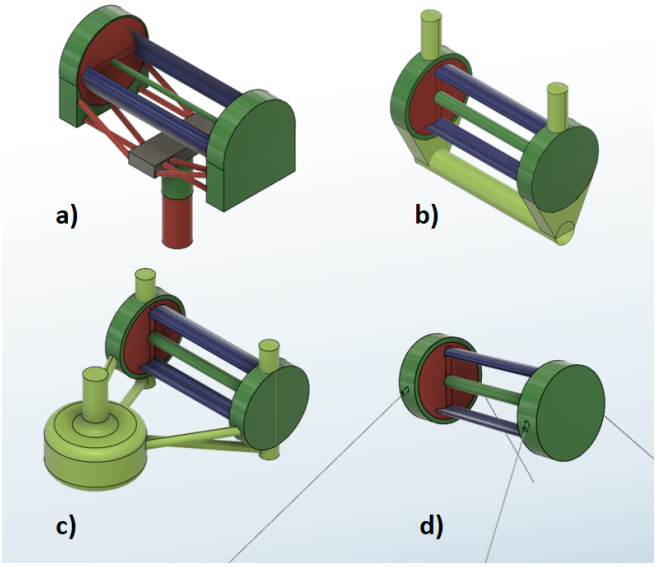

Fig. 1. Baseline configurations of LiftWEC cyclorotors [3], [11]: a) Tower LiftWEC, b) Spar LiftWEC, c) Semi-sub LiftWEC, d) Tension leg platform LiftWEC

However, such a promising LCoE value is estimated under an assumption of the implemented optimal control strategy [18]–[20]. Real time control for cyclorotor WECs is a challenging problem due to the high nonlinearity of even simplified mathematical models of interaction between the waves and hydrofoils [6], [18], [21].

An analysis of 2D tests of the scaled LiftWEC prototype were published in [7], [22]. The authors derived lift and drag coefficients, and studied the influences of unsteady effects. However, due to the size and specification of the 2D experimental setup, there was no positive mechanical power generation, on average, within the duration of the experiments recorded.

This article is dedicated to analysis of the new results of 3D tests of 1:20 scaled LiftEC prototype conducted at École Centrale de Nantes (ECN), France in 2022 [23], [24]. The tests show positive mechanical power generation with recorded wave power extraction efficiency up to 21.1%. Our goal is to identify the optimal conditions for power generation and determine the problems which need to be solved for further development of the technology and real-time control implementation.

Section II is dedicated to the mathematical point-vortex model for cyclorotor based WEC which will be used for the experimental data analysis. In Section III, the authors present performance metrics and the

This project has received funding from the European Union's Horizon 2020 research and innovation programme under grant agreement No. 851885. This work was supported by Science Foundation Ireland under Grant number 20/US/3687.

A. Ermakov and J.V. Ringwood are with Centre for Ocean Energy Research, Maynooth University, Ireland (e-mail: andrei.ermakov@mu.ie).

F. Thiebaut is with Ecole Centrale de Nantes, France (e-mail: florent.thiebaut@ec-nantes.fr).

Digital Object Identifier:
https://doi.org/10.36688/ewtec-2023-paper-id

developed control strategy for optimal cyclorotor rotational velocity. In Section IV, the authors describe experimental testing of a 3D LiftWEC prototype [23], [24] conducted at École Centrale de Nantes (ECN), France in 2022. In Section V, the authors analyse the experimental tests and assess the optimal conditions for which maximum rotor efficiency was achieved. The Conclusions (Section VI) are dedicated to discussion of the experimental results and important findings for the further development of cyclorotor WECs.

II. Analytical control oriented model for cyclorotor WECs

The analysis of the experimental data and development of real-time control strategies are based on the 2D point-vortex model [21], [25]. The selected mathematical model has been successfully validated against the Atargis experimental tests [26], [27] in terms of waves generated by the rotating foils in [25], [28]. It has also been validated against the tests of a 2D scaled LiftWEC prototype [29], [30] and CFD simulation results [31], in terms of the generation of tangential and radial forces, in [7], [8], [22]. The detailed diagram of the mathematical model of a cyclorotor with two hydrofoils is presented in the Fig. 2.

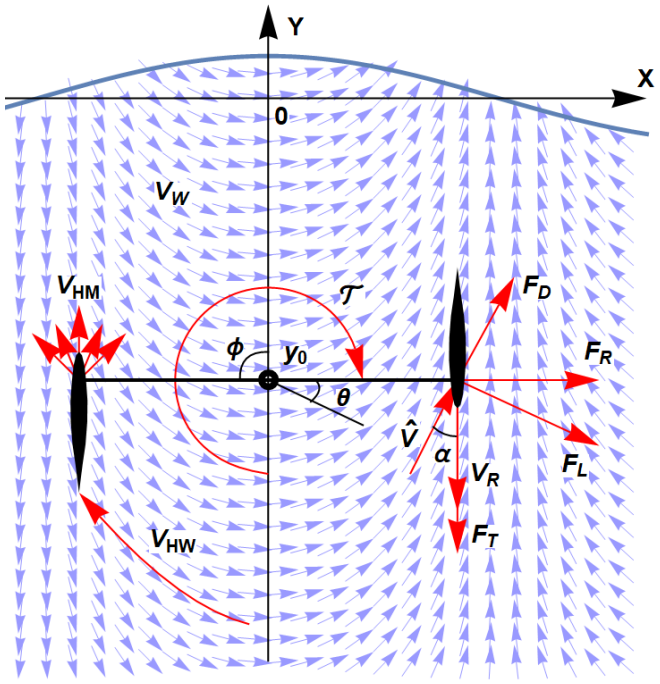

Fig. 2. Analytical model for cyclorotor WECs: θ - the polar angle position of the hydrofoil, y_0 - the submergence of the rotor shaft, V_W - the wave-induced fluid velocity, V_R - the instantaneous velocity of the foil, $\hat{V}$ - the overall relative foil/fluid velocity, V_{HM} - the instantaneous radiation from the foil, V_{HW} - the wakes left behind the hydrofoil, α - the attack angle, F_L, F_D, F_T, F_R - the lift, drag, tangential, and radial forces, $\mathcal{T}$ - the torque on the rotor shaft, and ϕ - the relative phase between the first hydrofoil ($i = 1$) at the top dead centre position and the wave crest location above the cyclorotor shaft.

In the case of a cyclorotor with two hydrofoils, the position (x_i, y_i) of the hydrofoil i, can be determined as:

$$x_i(t) = R\sin(\theta(t) + \pi(i-1)) \quad (1)$$

$$y_i(t) = y_0 + R\cos(\theta(t) + \pi(i-1)), \quad (2)$$

where $\theta(t)$ is the polar angle of the hydrofoil position at time instant t, R is the rotor radius and y_0 is the submergence depth of the rotor centre.

Then, the instantaneous rotational velocity $\mathbf{V_R}$, resolved into Cartesian coordinates, can be found as the time derivative of position as:

$$V_{Rx_i}(t) = R\dot{\theta}(t)\cos(\theta(t) + \pi(i-1)) \quad (3)$$

$$V_{Ry_i}(t) = -R\dot{\theta}(t)\sin(\theta(t) + \pi(i-1)), \quad (4)$$

where $\dot{\theta}(t)$ is the angular velocity.

Cyclorotor rotation is considered in monochromatic waves, which can be modeled as potential Airy waves [7]:

$$\Phi_W = \frac{Hg}{2\omega} e^{ky}\sin(kx - \omega t + \phi), \quad (5)$$

where H is the wave height, g is gravitational acceleration, ω is the wave frequency, k is the wave number, ϕ is the relative phase between the first hydrofoil i=1, at top dead centre position, and the wave crest location above the cyclorotor shaft.

Then, the wave induced fluid particle circulation velocity $\mathbf{V_W}$ can be found as the gradient of the potential (5):

$$\mathbf{V_W} = \nabla\mathbf{\Phi_W}, \quad (6)$$

The wakes generated by the hydrofoils can be approximated as the waves radiated by a moving point-vortex, which has the following complex potential [7]:

$$\mathcal{F}(z,t) = \frac{\Gamma(t)}{2\pi\,\mathrm{i}} Log\left[\frac{z - c(t)}{z - \tilde{c}(t)}\right] - \frac{2\mathrm{i}\sqrt{g}}{\pi}\int_0^t \frac{\Gamma(\tau)}{\sqrt{\mathrm{i}(z - \tilde{c}(\tau))}} D\left[\frac{\sqrt{g}(t-\tau)}{2\sqrt{\mathrm{i}(z - \tilde{c}(\tau))}}\right] d\tau \quad (7)$$

where $z = x + \mathrm{i}y$ is the coordinate on the complex plane, $c(t) = x(t) + \mathrm{i}y(t)$ is the position of the of the point-vortex, $\tilde{c}(t)$ is the complex conjugate of the position on the complex plane, and $D(x)$ is the Dawson function [32]:

$$D(x) = e^{-x^2}\int_0^x e^{y^2} dy. \quad (8)$$

The intensity of the circulation of the point-source vortex Γ is proportional to the lift force F_L generated on the hydrofoil [33]:

$$\Gamma = F_L/(\rho|\hat{V}|) = \frac{1}{2} C_L(\alpha)\,|\hat{V}|\,C, \quad (9)$$

where $\hat{V}$ is the relative foil/fluid velocity, ρ is the water density, C is the hydrofoil chord length, $C_L(\alpha)$ is the lift coefficient [34], and α is the angle of attack.

The velocity components of the waves radiated by the rotating hydrofoil can be found as the partial derivative of the complex potential:

$$\mathbf{V_H} = \frac{\partial\mathcal{F}(\mathbf{z},\mathbf{t})}{\partial\mathbf{z}} = (\mathbf{V_H})_\mathbf{x} - \mathrm{i}\,(\mathbf{V_H})_\mathbf{y}\,. \quad (10)$$

The obtained velocity vector components can be separated into the instantaneous radiated waves $\mathbf{V_{HM}}$

(the first term of the equation (7)), and wakes $\mathbf{V_{HW}}$, which are left behind the hydrofoil (the integral part of equation (7)):

$$\mathbf{V_H} = \mathbf{V_{HM}} + \mathbf{V_{HW}}, \tag{11}$$

Thus, the relative foil/fluid velocity for the hydrofoil i can be calculated using:

$$\hat{\mathbf{V}}_\mathbf{i} = \mathbf{V_{W_i}} - \mathbf{V_{R_i}} + \mathbf{V_{HW_i}} + \mathbf{V_{HM_j}} + \mathbf{V_{HW_j}}, \tag{12}$$

where components with the index j correspond to the wave radiation from opposite hydrofoil and should be omitted in the case of a single hydrofoil cyclorotor. The vector $\mathbf{V_{R_i}}$ is taken with a negative sign since the direction of the water flow is the opposite to the instantaneous rotational velocity of the foil. Additionally, it is not possible define the instantaneous radiated waves $\mathbf{V_{HW}}_i$ in the immediate vicinity of the point source i due to the singularity highlighted in [35].

The inclusion of the near fluid velocity field permits correction of the estimate of the angle of attack for the rotor foil:

$$\alpha_i(t) = \arcsin\left(\frac{(V_{R_i})_x * (\hat{V}_i)_y - (V_{R_i})_y * (\hat{V}_i)_x}{|V_{R_i}||\hat{V}_i|}\right) + \gamma_i, \tag{13}$$

where γ_i is the pitch angle of hydrofoil i.

Then, the tangential forces F_T, generated on each hydrofoil, can be found as:

$$\begin{aligned} F_{T_i} = \quad & \frac{1}{2}\,\rho(C_L(\alpha_i)\sin(\alpha_i - \gamma_i) - \\ & C_D(\alpha_i)\cos(\alpha_i - \gamma_i))|\hat{V}|^2\, C\, S, \end{aligned} \tag{14}$$

where S is the span of the hydrofoils, $C_L(\alpha_i)$ and $C_D(\alpha_i)$ are lift and drag coefficients, respectively, which can be approximated as lift and drag coefficients obtained for aerofoils in [34].

III. Control system formulation and solution

A. Performance function

The tangential forces F_{T_i} generated on the hydrofoils create a mechanical torque $\mathcal{T}$ on the rotor shaft, which can be absorbed by a rotational generator. Based on the angular version of Newton's second law, the mechanical torque $\mathcal{T}$ torque can be evaluated using:

$$\mathcal{T} = (F_{T_1} + F_{T_2})R - I\ddot{\theta}(t), \tag{15}$$

where I is the moment of inertia of the rotor, and $\ddot{\theta}(t)$ is the angular acceleration.

Then, the mechanical power generated within time interval from $[T_0, T_N]$ can be evaluated as:

$$P_{Shaft} = \frac{1}{(T_N - T_0)}\int_{T_0}^{T_N} \mathcal{T}(t)\dot{\theta}(t)dt. \tag{16}$$

The hydrodynamic efficiency of the tested cyclorotor is assessed in terms of the traditional metric for wave energy converters (WECs) - the capture width ratio (CWR). This efficiency metric, denoted as η, reflects the fraction of wave power flowing through the device that is absorbed by the device [36]:

$$\eta = \frac{P_{Shaft}}{P_{Airy} * S} * 100\%, \tag{17}$$

where S is the span of the cyclorotor foils, P_{Airy} is the power of the monochromatic Airy waves, which can be evaluated as:

$$P_{Airy} = \frac{1}{32\pi}\rho g^2 H^2 T, \tag{18}$$

where T is the wave period.

B. Optimal control strategy

The 3D LiftWEC scaled prototype assessments include tests of prescribed rotational velocity control strategies. The tested rotational velocity changes are based on the analytical control solutions presented in [18]–[20], which show, that the variation of the rotational velocity $\dot{\theta}(t)$, within the period of monochromatic wave T, permits an increase of the power production compared to a constant rotational velocity strategy (for which $\dot{\theta} = \omega$). In the case of monochromatic waves, the control goal of maximisation of generated mechanical power can be presented in the following form:

$$Max \quad \frac{R}{T}\int_{T_K}^{T_{K+1}} (F_{T_1} + F_{T_2})\,\dot{\theta}(t)dt, \tag{19}$$

where K is the period index of the synchronous rotation of the cyclorotor with the waves. We select $K = 8$, since as it was shown in [18], that after eight rotational periods of the rotor in phase with the incident waves, all hydrodynamic and mechanical processes became periodic. The influence of the moment of inertia I in (15) can be ignored in (19), for the constant velocity cases, or periodic solutions on the selected time interval $\dot{\theta}(T_{K+1}) = \dot{\theta}(T_K)$.

According to the optimal control method presented in [18], the average angular velocity of a cyclorotor WEC, within the wave period T, must be equal to the wave frequency ω, in order to achieve a periodic solution within T. Then, the optimal position of the cyclorotor hydrofoils $\theta(t)$, within the period of a monochromatic wave, can be found in the form of the following Fourier series:

$$\theta(t) = \omega\, t + \sum_{i=1}^{m} a_i \cos\left(\frac{2\pi\, t}{T} i\right) + b_i \sin\left(\frac{2\pi\, t}{T} i\right) \tag{20}$$

where the coefficients a_i and b_i need to be determined from the optimisation problem in (19).

The optimal angular velocity $\dot{\theta}$ and acceleration $\ddot{\theta}$ can be obtained by differentiation of the series in (20) with respect to time t. Thus, the mechanical energy which can be generated in monochromatic waves can be evaluated by substitution of (20) into the functional (19). It was shown, in [18], that m=15 time series coefficients is sufficient to achieve convergence of the solution.

The functional (19) is discretized using a finite difference method and all model equations are programmed in Python. The optimal coefficients a_i and b_i were

determined numerically using a global optimisation algorithm [18]. The angular velocity was limited $0.75\omega < \dot{\theta} < 1.25\omega$ in order to align with capabilities of the experiment PTO system. The obtained time profiles of the optimal foil position, within each period of the monochromatic waves, were submitted for testing.

IV. Experimental tests of 3D LiftWEC prototype

The 1:20 scale 3D prototype of the LiftWEC cyclorotor (Fig. 3) was designed, built, assembled and commissioned by Ecole Centrale Nantes (ECN), France [23], [24]. The created cyclorotor has radius R=0.3m, central shaft submergence y_0=-0.6m, and allows installation of one or two curved hydrofoils NACA0015 with chord length C=0.3m and span S=1.49m. The hydrofoil pitch angles γ_i were adjusted manually between tests. The angular velocity of the rotor was controlled using a power take off (PTO) system, consisting of an electrical motor which can be controlled in both angular speed $\dot{\theta}$ and torque $\mathcal{T}$.

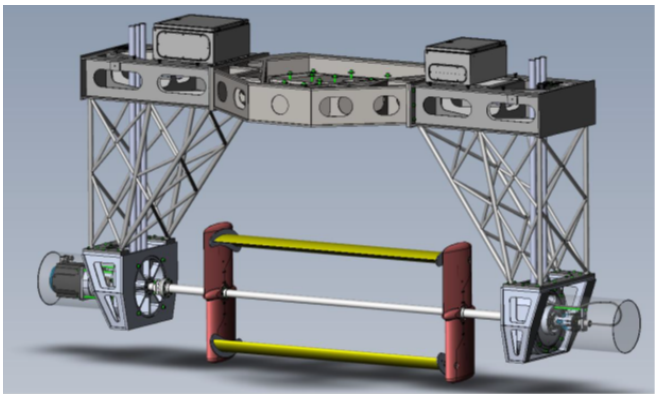

Fig. 3. Experimental scaled prototype of a LiftWEC with two hydrofoils

Experimental testing of the 3D scaled prototype, in regular and irregular waves, was conducted in the Hydraulic and Offshore Engineering wave Tank (HOET) in September and October 2022. Ten wave gauges were used for wave calibration before the experiments, and for free surface elevation measurement around the cyclorotor during tests. Sensors installed on the rotor allow measurement of the rotor angular position, radial and tangential loads on the foils, the torque generated on the main shaft, as well as the position of the hexapod holding the model. Sensor cells on the rotor arms, which allow measurement of radial and tangential loads, were covered by the struts (see Fig. 4). The shape of the struts is based on NACA0021 profiles to achieve low drag. Fig. 4 also shows the end-plates, which were installed in order to avoid tip vortices influences.

The model design details are described in a LiftWEC project deliverable [23], and data which was measured during more than 600 experimental tests is published in open access on Zenodo [24]. Indexation of the tests presented here is the same as in the published dataset. More details on the experimental test campaign is available in a LiftWEC deliverable, in open access on Zenodo [37]

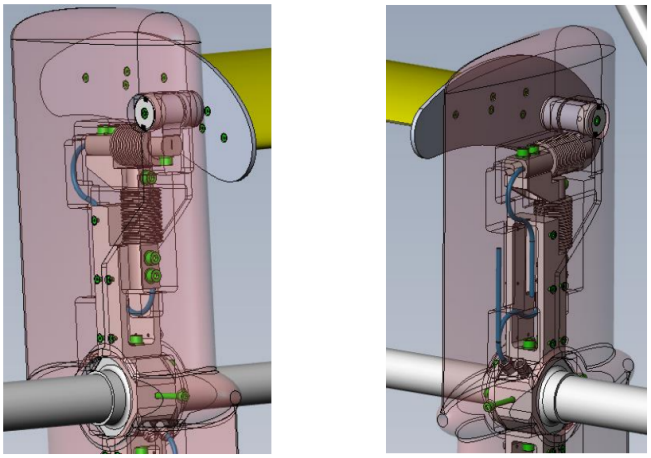

Fig. 4. Struts, end-plates, and sensors on the rotor arms.

V. Analysis of the experimental tests

A. Analysis of optimal conditions for power production

This subsection is dedicated to analysis of selected tests of the cyclorotor with different hydrofoil configurations with constant rotational velocity $\dot{\theta} = \omega$, and different phases ϕ in a monochromatic wave H=0.15m, T=2s and P_{Airy}=43W/m. The average efficiency η of each configuration is assessed over 20 wave periods, from T_0=20s to T_N=60s, using (17). The results of the efficiency assessment are presented in Table 1. The rows of the table corresponds to the different phase values ϕ, between the first hydrofoil position (1),(2) and the wave crest (5). It is seen, that the maximum efficiency corresponds to the cases when the first hydrofoil has $\phi = 270^o$ phase with the incoming wave. Tests 190-201 conducted for Configuration I study rotation of a single hydrofoil with pitch angle $\gamma_1 = -4^o$ without end-plates, while Tests 288-294 for Configuration II were conducted in the same experimental conditions, but with end-plates installed on the hydrofoil (see Fig. 3). The end-plates are designed to minimise the influence of tip-vortices, reduce the dynamic drag, and increase the lift force generation. During the conducted tests, the maximum tangential force recorded for Configuration I (Test 190, without end-plates) is F_T =10.23N but, after the installation of end-plates (Test 288), it reached F_T =10.49N [24]. So, it was decided to keep the end-plates installed for all consequent tests. However, post analysis of the experimental data has shown that end-plates have a negative influence on the rotor efficiency (see Table I). This conclusion regarding the losses associated with end-plates is in agreement with the results obtained from experimental tests and numerical simulations of cross-flow turbines in a mean flow [38].

The assessments presented for Configurations I and II show how sensitive the rotor efficiency is to the optimal rotor phase with respect to the wave crest. A positive shift of $+45^o$ from the optimal phase $\phi = 270^o$ results in no power production, and the experimental setup only expends energy to maintain hydrofoil rotation. A negative shift of -45^o from the optimal phase causes a loss of 2/3 of the foil efficiency without

TABLE I
THE DEPENDENCE OF AVERAGE POWER PRODUCTION WITHIN THE WAVE PERIOD ON THE OPTIMAL PHASE WITH MONOCHROMATIC WAVE H=0.15M, T=2S, FOR CYCLOROTORS WITH DIFFERENT CONFIGURATIONS OF HYDROFOILS.

	Configuration I		Configuration II		Configuration III		Configuration IV	
	Single foil, No Endplates, Pitch=-4		Single foil, Endplates, Pitch=-4		Single foil, Endplates, Pitch=0		Two foils, Endplates, Pitch=0	
Phase ϕ	Test №	Efficiency(%)	Test №	Efficiency(%)	Test №	Efficiency(%)	Test №	Efficiency(%)
0	199	-12.36	294	-11.53	388	-9.95	540	-15.67
90	201	3.07			497	7.01		
180	197	-8.32	292	-10.32	386	-12.32	538	-15.66
225	196	3.36	291	1.78	385	6.22	537	9.93
270	190	10.1	288	9.1	382	16.1	534	21.1
315	198	-4.14	293	-6.57	387	1.64	539	-2.61

end-plates, and 3/4 for a foil with end-plates. The decrease in efficiency can be explained by the changes in the direction of the relative foil/fluid velocity $\hat{V}$ and ranges of angles of attack α which hydrofoil experiences by following the prescribed path. Thus, in Test 201, the hydrofoil has relative phase of $\phi = 90^o$, which is a counter phase to the optimal phase of $\phi = 270^o$ (Test 190). As a result, during Test 201, the hydrofoil experiences the same range of angles of attack as in Test 190, but with opposite signs. The difference in the efficiency can be explained by the asymmetric shape of the curved hydrofoil.

The tests of Configuration III were assessments of a single hydrofoil with a neutral (zero) relative pitch angle $\gamma_1 = 0$. An increase in pitch angle by $+4^o$, compared to the tests of the Configurations I and II, leads to an increase in the number of phases for which power production was recorded. An increase of the pitch angle also allows an almost doubling of power production for the case of optimal phase (Test 382). However, the range of the angles of attack experienced by the foil also shifted closer to the stall point, for which flow separation was observed during the experimental tests. Despite the increase in power production, the flow separation also leads to a significant increase in the radial force and, as a result, a corresponding increase in structural loading. Such loads cause fatigue of the structure, increase in the operational costs of the cyclorotor WEC and its LCoE. That is why stall angles should be avoided.

Configuration IV has two hydrofoils, both with zero pitch angles $\gamma_1 = \gamma_2 = 0$. Its maximum efficiency η=21.1% is achieved in Test 534, which has rotation with the optimal phase $\phi = 270^o$ for the first foil and opposite phase $\phi = 90^o$ for the second foil. If we ignore any interaction between two hydrofoils, Test 534 can be considered as the sum of separate Tests 382 and 497 for single foils. However, the efficiency which was recorded during Test 534, P_{534}=21.1% is less than the sum of the efficiencies in Tests 382 and 497, $P_{382} + P_{497}$=23.2%. The 2.1% of efficiency loss can be explained by the fact that the hydrofoils operate within the wakes left by each other. The wakes cause significant disturbance in the relative foil fluid velocity field $\hat{V}$ and influence the actual angles of attack α. That is why it is recommended to limit the number of rotor hydrofoils to two.

B. Implementation of the optimal control strategies

The 3D experimental tests of the scaled LiftWEC prototype also include tests of the variable velocity control strategies. The control strategies were developed with the use of the control solution methods described in Subsection V-A using lift and drag coefficients for aerofoils NACA0015 [34]. It was planned to use prescribed control, which controls the hydrofoil position θ within the period T of the monochromatic waves. It was expected to achieve at least approximately 10% increase in mechanical power generation.

Contrary to expectations, during the test campaign, it became apparent that the experimental PTO cannot exactly control the position of the foil, but can only change the rotational speed $\dot{\theta}$. The speed profiles also cannot be controlled accurately (i.e. the speed does not exactly follow the optimal setpoint), and there is a significant difference between the planned end actual foil behaviour within the monochromatic wave period (See Fig. 5).

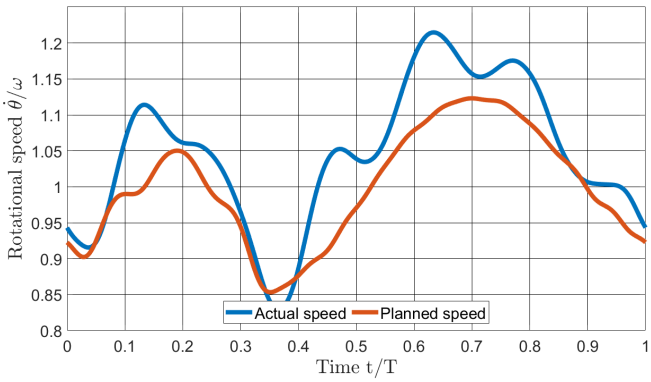

Fig. 5. The planed and actual rotational speeds of the foil during Test 484.

Fig. 5 illustrates the difference between the planned and actual rotational speed for a single hydrofoil with pitch $\gamma = 4^o$ which was tested in monochromatic waves, with H=0.15 and T=2s, in Test 484. As can be seen from Fig. 5, the actual rotational speed exceeds the planned speed, which leads to a significant increase in phase difference by $\Delta\phi = 16.68^o$ between the foil and incoming wave, during each of rotational periods. As a

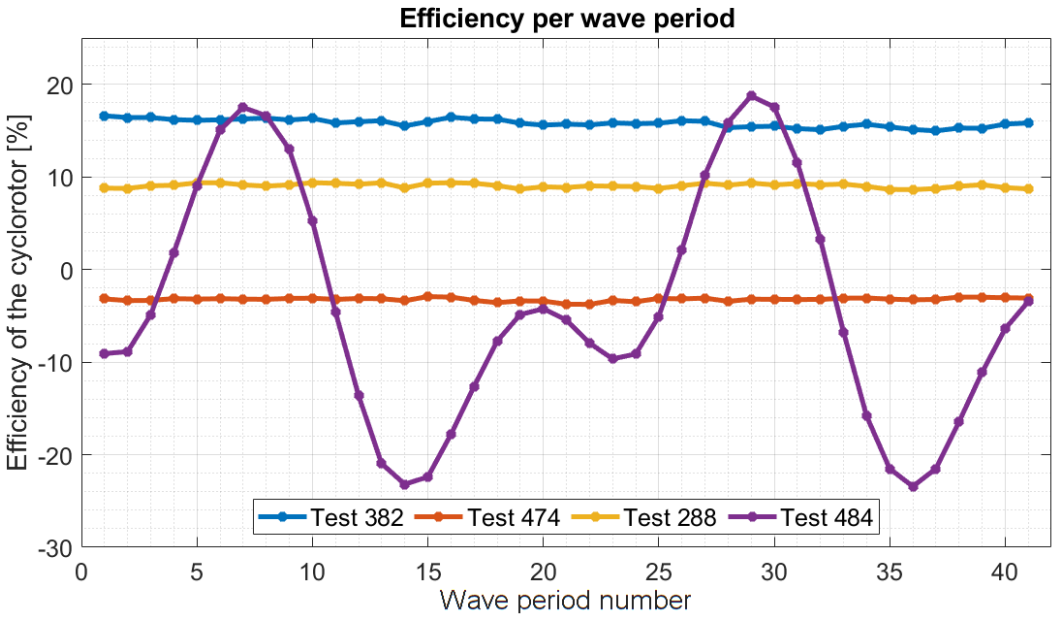

Fig. 6. The efficiency of the cyclorotor for constant and variable speed control strategies

result, there are only a few short time intervals where the hydrofoil is relatively close to the expected position (optimal conditions) within the wave period.

Fig. 6 shows a comparison of the rotor efficiency η for various full periods of monochromatic waves with T=2s and H=0.15m. The blue, red and yellow lines correspond to Tests 382, 288 and 474, respectively, where the foil has constant velocity $\dot{\theta} = \omega$, relative foil/wave phase of $\phi_{382} = 270^o$, $\phi_{288} = 270^o$, $\phi_{474} = 0^o$, and pitch angles $\gamma_{382} = 0^o$, $\gamma_{288} = -4^o$, $\gamma_{474} = 4^o$, respectively. The purple line corresponds to Test 484, where a variable rotational velocity (see Fig. 5) was tested for a single hydrofoil with pitch of $\gamma = 4^o$. It is noticeable, from Fig 6, that, during periods 19-21, the foil has relative phase ϕ close to 90^o which is very close to conditions of Test 474. However, the foil requires more energy for rotation because of inaccurate phase and the variable velocity profile. After 10 cycles, the phase of the foil is shifted by a total of 166.8^o and the foil obtains a close to optimal phase $\phi = 270^o$. It allows for the generation of even more energy compared to Test 382, due to the variable velocity and larger value of pitch angle. Thus, it is clear that, only during cycles 7, 8, 28, 29 and 30, the phase ϕ between the foil and wave is optimal, and the foil generates 5-10% more energy compared to the best case of constant velocity.

When manufacturing and testing a bespoke experimental model, it is rare not to experience some unplanned situations, especially when the model is associated with a novel concept. The problems experienced have shown that the PTO system for LiftWEC will require a stronger and more accurate generator/motor to reproduce the prescribed velocity profile. Nevertheless, the data generated from this test was also used for further control-oriented model validation and, when optimal velocity tracking was achieved, the power capture increase was consistent with model predictions.

VI. Conclusions

In general, the 3D LiftWEC scaled prototype test campaign was successful. The assessments of the experimental tests have shown capture width ratio efficiency up to 21.1%. Further development of the cyclorotor WEC design and control strategy will definitely increase the device efficiency.

The first problem which must be addressed is optimisation of hydrofoil profile. The tested aerofoils NACA0015 struggle to maintain attached flow during rotation in waves. New specifically designed hydrofoils will increase the range of angles of attack for operations, generation of lift forces, as well as decrease drag effects. The experimental foils also were tested for a relatively small Reynolds number, so it is expected to see an increase in the lift coefficients for the much larger Reynolds numbers in which a full scale prototype will work. In addition to larger radius and speeds, a full scale prototype will have a larger hydrofoils span, which will also increase the generation of lift forces and, as a result, the efficiency of the device. It has been shown that an increase in the number of hydrofoils will not result in a linear increase in performance, as the hydrofoils will operate within the strong wakes generated by each other.

The experimental tests confirmed the high sensitivity of the power production to the hydrofoil phase ϕ relative to the incoming wave. A shift of $\pm 45^0$ from the optimal phase leads to a significant loss of power production. That is the main reason why the rotor *position* must be controlled in real time. Correct hydrofoil pitch angle is also very important for the maintenance of the optimal angle of attack. It is shown that a shift in the pitch angle of $\pm 4^o$ can double energy production. On the other hand, as shown in [7] and [22], the large values of angle of attack ($\alpha > 14^o$) cause a stall effect, which significantly increases the structural loads and leads to the fatigue and damage of the cyclorotor. That is why it is important to control cyclorotor WECs in

real time, in both pitch and velocity. The real time control strategy must be able to identify the optimal phase, rotational velocity and pitch angle for much more complex fluid velocity fields corresponding to panchromatic waves in real sea states.

While the conducted analysis covers only four cyclorotor configurations and one type of monochromatic waves, the methodology developed and presented in this paper can be used for analysis of the data from more than 400 experimental tests of the scales 3D LiftWEC prototype. These test results are published in open access in [24], [37]. The experimental test data include: a) wave calibrations tests; b) substructure drag and motion tests; c) tests of cyclorotors with one or two hydrofoils with different constant hydrofoil pitch angles γ_i, in air, still water and various monochromatic and panchromatic waves; d) tests of different rotational speeds $\dot{\theta}$, submergence depths y_0 and phases with the wave crest ϕ in monochromatic waves; e) free wheeling tests;

Despite limited success in these first tests of prescribed control of rotational velocity, the obtained results can be used for further development of the real time control for cyclorotor-based WECs. It is clear that the rotor requires actuators which will allow accurate tracking of the optimal phase, velocity and angle of attack. Feedforward (precomputed) control was not ideal, due to inaccuracies in the system, including lack of synchronisation with the actual free surface in the tank. In addition, an accurate predictor of the relative foil fluid velocity and an estimator for the cyclorotor state must be developed for real-time operation in panchromatic waves.

Nevertheless, the experimental tests confirmed many analytical hypotheses which are used for full-scale device performance prediction. The performance analysis conducted within the LiftWEC project, supported by numerical, physical and economical modeling conducted by the consortium of 10 industry and academia partners' permitted the estimation of LCoE at $\sim$ 140 €/MWh [10]. It creates motivation for the further study and development of cyclorotor-based WEC technology.

REFERENCES

[1] A. Ermakov and J. V. Ringwood, "Rotors for wave energy conversion—practice and possibilities," *IET Renewable Power Generation*, vol. 15, p. 3091–3108, 2021.

[2] M. Folley and T. Whittaker, "Lift-based wave energy converters – an analysis of their potential," in *Proceedings of the 13th European Wave and Tidal Energy Conference, Napoli, Italy*, 2019.

[3] LiftWEC Consortium, Available: https://liftwec.com/ [Accessed: 10-March-2023], 2023.

[4] Atargis, the Energy Corporation, Available: https://atargis.com// [Accessed: 19-April-2023], 2023.

[5] K. C. Chitale, C. Fagley, A. Mohtat, and S. G. Siegel, "Numerical evaluation of climate scatter performance of a cycloidal wave energy converter," *International Marine Energy Journal*, vol. 5 (3), pp. 315—-326, 2022.

[6] S. G. Siegel, "Numerical benchmarking study of a cycloidal wave energy converter," *Renewable Energy*, vol. 134, pp. 390–405, 2019.

[7] A. Ermakov, F. Thiebaut, G. S. Payne, and J. V. Ringwood, "Validation of a control-oriented point vortex model for a cyclorotor-based wave energy device," *Journal of Fluids and Structures*, vol. 119, 2023.

[8] A. Arredondo-Galeana, G. Olbert, W. Shi, and F. Brennan, "Near wake hydrodynamics and structural design of a single foil cycloidal rotor in regular waves," *Renewable Energy*, vol. 206, pp. 1020–1035, 2023.

[9] J. Fernández Chozas, A. Tetu, and A. Arredondo-Galeana, "A parametric cost model for the initial techno-economic assessment of lift-force based wave energy converters," in *Proceedings of 14th European Wave and Tidal Energy Conference, paper #2005, Plymouth, UK*, 2021.

[10] K. Nielsen, J. Fernandez Chozas, R. Pascal, and F. Ferri, "LiftWEC project deliverable D8.6: LCoE of the final configuration," https://liftwec.com/wp08-cost-of-energy/ [Accessed: 19-April-2023], 2023.

[11] P. Lamont-Kane, M. Folley, R. Pascal, J. F. Chozas, and K. Neilson, "LiftWEC project deliverable D2.10 Assessment of baseline configurations and specification of final configuration," https://liftwec.com/wp02-concept-development-evaluation/ [Accessed: 30-March-2023], 2023.

[12] B. Guo and J. V. Ringwood, "A review of wave energy technology from a research and commercial perspective," *IET Renewable Power Generation*, vol. 15, no. 14, pp. 3065–3090, 2021.

[13] M. Folley and P. Lamont-Kane, "Optimum wave regime for lift-based wave energy converters," in *Proceedings of 14th European Wave and Tidal Energy Conference, paper #1914, Plymouth, UK*, 2021.

[14] P. Lamont-Kane, M. Folley, C. Frost, and T. Whittaker, "Preliminary investigations into the hydrodynamic performance of lift based wecs," in *Proceedings of 14th European Wave and Tidal Energy Conference, paper #2074, Plymouth, UK*, 2021.

[15] A. Arredondo-Galeana, W. Shi, G. Olbert, M. Scharf, A. Ermakov, J. V. Ringwood, and F. Brennan, "A methodology for the structural design of LiftWEC: A wave-bladed cyclorotor," in *Proceedings of 14th European Wave and Tidal Energy Conference, paper #1967, Plymouth, UK*, 2021.

[16] A. Arredondo-Galeana, A. Ermakov, W. Shi, J. V. Ringwood, and F. Brennan, "Control strategies for power enhancement and fatigue damage mitigation of wave cycloidal rotors," Available: https://papers.ssrn.com/sol3/papers.cfm?abstract_id=4346306 [Accessed: 19-April-2023], 2023.

[17] A. Martinez and G. Iglesias, "Mapping of the levelised cost of energy for floating offshore wind in the European Atlantic," *Renewable and Sustainable Energy Reviews*, vol. 154, p. 111889, 2022.

[18] A. Ermakov, A. Marie, and J. V. Ringwood, "Optimal control of pitch and rotational velocity for a cyclorotor wave energy device," *IEEE Transactions on Sustainable Energy*, vol. 13, no. 3, pp. 1631–1640, 2022.

[19] A. Ermakov, A. Marie, and J. Ringwood, "Some fundamental results for cyclorotor wave energy converters for optimum power capture," *IEEE Transactions on Sustainable Energy*, vol. 13, pp. 1869–1872, 2022.

[20] J. V. Ringwood and A. Ermakov, "Energy-maximising control philosophy for a cyclorotor wave energy device," in *41st International Conference on Ocean, Offshore & Arctic Engineering (OMAE), Hamburg*, no. 80990. American Society of Mechanical Engineers, 2022.

[21] A. Ermakov and J. V. Ringwood, "Development of an analytical model for a cyclorotor wave energy device," in *Proceedings of 14th European Wave and Tidal Energy Conference, paper #1885, Plymouth, UK*, 2021.

[22] A. Ermakov, F. Thiebaut, G. S. Payne, and J. V. Ringwood, "Analytical study of pre-stall hydrofoil experimental data for a cyclorotor-based wave energy converter," in *Proceedings of OCEANS 2023, Limerick, Ireland*, 2023.

[23] F. Thiebaut, S. Haquin, M. Weber, S. Lamber, B. Pettinotti, and M. Folley, "LiftWEC project deliverable D4.5: 3D scale model of the final LiftWEC concept selected," https://liftwec.com/wp04-physical-modelling/ [Accessed: 19-April-2023], 2023.

[24] F. Thiebaut, G. Payne, S. Haquin, M. Weber, S. Lamber, and B. Pettinotti, "LiftWEC project deliverable D4.7: Open access experimental data from 3D scale model," https://doi.org/10.5281/zenodo.7669668. [Accessed: 19-April-2023], 2023.

[25] A. Ermakov and J. V. Ringwood, "A control-orientated analytical model for a cyclorotor wave energy device with n hydrofoils," *Journal of Ocean Engineering and Marine Energy*, vol. 7, pp. 201–210, 2021.

[26] C. P. Fagley, J. J. Seidel, and S. G. Siegel, "Computational investigation of irregular wave cancellation using a cycloidal wave energy converter," in *Intl. Conf. on Offshore Mechanics and Arctic Eng. (OMAE), Rio de Janeiro*, vol. 44946, 2012, pp. 351–358.

[27] ——, "Wave cancellation experiments using a 1:10 scale cycloidal wave energy converter," in *Proc. 1st Asian Wave and Tidal Energy Conf., Jeju Island, Korea*, 2012.

[28] A. Ermakov and J. V. Ringwood, "A validated analytical model for a cyclorotor wave energy device," *International Marine Energy Journal*, vol. 5, no. 2, pp. 201–208, 2022.

[29] F. Thiebaut, G. Payne, S. Haquin, M. Weber, S. Lamber, and B. Pettinotti, "LiftWEC project deliverable D4.3 Open access experimental data from 2D scale model," https://doi.org/10.5281/zenodo.5534471 [Accessed: 30-March-2023], 2021.

[30] F. Thiebaut and G. Payne, "LiftWEC project deliverable D4.4 Report on Physical Modelling of 2D LiftWEC Concepts," https://cordis.europa.eu/project/id/851885. [Accessed: 30-March-2023], 2021.

[31] G. Olbert, M. Scharf, S. Felten, and M. Abdel-Maksoud, "Comparison of rans and potential flow theory based simulations of a cyclorotor type wave energy converter in regular waves," in *Proceedings of 14th European Wave and Tidal Energy Conference, Plymouth, UK*, 2021.

[32] H. G. Dawson, "On the numerical value of $\int_0^h e^{x^2}\,dx$," *Proceedings of the London Mathematical Society*, vol. s1-29 (1), pp. 519–522, 1897.

[33] G. K. Batchelor, *An Introduction to Fluid Dynamics*. Cambridge University Press, 1967.

[34] R. Sheldahl and P. Klimas, *Aerodynamic characteristics of seven symmetrical airfoil sections through 180-degree angle of attack for use in aerodynamic analysis of vertical axis wind turbines*. Sandia National Labs., Albuquerque, 1981.

[35] S. G. Siegel, T. Jeans, and T. E. McLaughlin, "Deep ocean wave energy conversion using a cycloidal turbine," *Applied Ocean Research*, vol. 33, no. 2, p. 110–119, 2011.

[36] A. Babarit, "A database of capture width ratio of wave energy converters," *Renewable Energy*, vol. 80, pp. 610–628, 2015.

[37] F. Thiebaut and G. Payne, "LiftWEC project deliverable D4.8: Report on physical modelling of 3D LiftWEC concepts," https://doi.org/10.5281/zenodo.7669625. [Accessed: 19-April-2023], 2023.

[38] R. Urbina, B. P. Epps, M. L. Peterson, and R. W. Kimball, "A dynamic stall model for analysis of cross-flow turbines using discrete vortex methods," *Renewable Energy*, vol. 130, pp. 1130–1145, 2019.